The influence of the structural defects on the physical properties of Er$_3$Fe$_5$O$_{12}$ ferrite-garnet

Kamaludin Abdulvakhidov [a],[*], Alexander Soldatov [a], Ivan Dmitrenko [b], Zhengyou Li [b], Suleiman Kallaev [c], Zairbek Omarov [c]

[a] The Smart Materials International Research Institute, Southern Federal University, Rostov-on-Don, Russia
[b] Faculty of Physics, Southern Federal University, Rostov-on-Don, Russia
[c] Institute of Physics, Dagestan Federal Research Centre of The Russian Academy of Sciences, Makhachkala, Russia

A B S T R A C T

It has been shown that structural defects can play a dominant role in the formation of the physical properties of ceramics. This paper presents the results of studying the physical properties of Er$_3$Fe$_5$O$_{12}$ (ErIG) powders and ceramics, containing the structural defects of various types. The formation of the structural defects in ErIG was achieved by the mechanical activation of pre-synthesized powders using Bridgman anvils, to which fixed shear strain and uniaxial pressures of various magnitudes were applied in the range of 40–320 MPa. The lower anvil rotated at the speed of 3 revolutions per hour (rph). The structural parameters of the mechanically activated powders and ceramics sintered from them were studied at room temperature by the X-ray method. The band gap was determined by the optical spectroscopy, the magnetic properties were estimated from the hysteresis loops and the dielectric properties and heat capacity were studied in the high-temperature range. It has been established that mechanical activation leads to a significant smearing of antiferrimagnetic transition and to a shift in the phase transition temperature to the low-temperature region.

Introduction

Ferromagnetic properties of ferrite-garnets were discovered in 1956 by Bertaut and Forrat [1] and Pauthenet [2] and, independently of them, by Geller and Gilleo in 1957 [3]. The formula of ferrite-garnets is R$_3$Fe$_5$O$_{12}$ where R is one of the rare earth elements or yttrium.

According to Nèel [4], the crystal structure of ferrite-garnets is a three-lattice structure, the Fe^{3+} ions are located in two of them (a and d), and the Re^{3+} ions are located in the third sublattice (c). All ferrite-garnets have approximately the same Curie points, which is explained by the fact that the Re^{3+} ions demonstrate very weak ferromagnetism; the interaction of the lattice c with d and a is small, so here the value of the Curie point is mainly determined by the interaction between the iron ions [5,6]. Ferrimagnetic ErIG studied in this work belongs to the rare-earth ferrite-garnets, which have a cubic symmetry with the *Ia3d* space group at room temperature. The unit cell contains 8 standard elements (160 elements): 96 – O^{2-}, 40 – Fe^{3+}, 24 – R^{3+}. The cations are located in the tetrahedra (24*d*), octahedra (16*a*), and dodecahedra (24*c*). The dodecahedral positions are occupied by the R^{3+} ions, the remaining positions are occupied by the Fe^{3+} ions. If the influence of M_c on M_a and M_d through the a − c and d − c interactions is neglected, then the total magnetic moment of the rare earth ferrite-garnet is determined by the formula [5]:

$$M = M_c - [M_d - M_a] \qquad (1)$$

This value equals to zero at the compensation temperature, T_c, which is 75 K for ErIG.

Many physical properties of ferrite-garnets depend on both the production methods and concentration and type of defects in them. Among the methods of the preparation, the following can be distinguished: chemical coprecipitation [7], pyrolysis of aerosol spraying [8], sol–gel method [9–11] and solid-phase reaction method [12–14].

In [10], the nanosized Er$_3$Fe$_5$O$_{12}$ was prepared by an aqueous sol–gel method. The minimum particle size according to SEM data was 75 nm. The relative amount of garnet phases in the sample Er$_3$Fe$_5$O$_{12}$ was evaluated using Mössbauer spectroscopy and confirmed by XRD measurements. This work established a correlation between the composition, particle size and magnetic properties.

In [11], the magnetic properties of Er-doped $Er_xY_{3−x}Fe_5O_{12}$ films obtained by sol–gel method were studied. The SEM photomicrograph showed that the particles had a strong agglomeration and the average particle size was about 82 nm. With the increase of Er concentration, the saturation magnetization (M_s) of the films decreased linearly. The authors attribute this to nanoparticle thin films. The results show that the coercivity H_c of $Er_xY_{3−x}Fe_5O_{12}$ ($0 \leq x \leq 2.5$) nanoparticles reaches the maximum when the particle size is 89 nm.

In [12], the structural parameters, Mössbauer spectroscopy, and hysteresis of $Er_3Fe_{5-x}Ga_xO_{12}$ ($0.0 \leq x \leq 0.8$) synthesized by solid-state reaction method were studied. When $x \leq 0.6$, XRD analysis, Mössbauer spectroscopy analysis, and the magnetic data are consistent with the assumption that Fe^{3+} ions are substituted by Ga^{3+} ions at tetrahedral sites in the samples. When $x = 0.8$, the partial substitution of Fe^{3+} ions for Ga^{3+} ions at octahedral sites splitted the octahedral component of Mössbauer spectrum into two. They found that the saturation magnetization decreases almost linearly as x increases, following a simple magnetic dilution model until $x = 0.6$, and deviating slightly from linear behavior at $x = 0.8$ due to partial substitution at the octahedral sites.

In another work [13], the dielectric relaxation properties of the polycrystalline ceramic $Er_3Fe_5O_{12}$ were studied in detail by measuring of dielectric modulus and impedance spectra. These ceramics were found to have a colossal dielectric constant (CDC) up to 10^6. At low temperature ($T < 600$ K), the dielectric relaxation at low frequency ($f \leq 50$ kHz) is mainly related to the Maxwell-Wagner effect. In addition, the authors consider that the low-frequency dielectric relaxation at high temperatures ($T \geq 600$ K) is due to the contribution of oxygen vacancy and grain boundaries, which is also considered to be the origin of CDC.

In another work [14], $Gd_{3−x}Er_xFe_5O_{12}$ powders were studied by the Mössbauer method at room temperature. The results show that the Mössbauer spectra were approximated by three magnetic sextets corresponding to iron ions (Fe^{3+}) in three different environments, two octahedral sites and one tetrahedral site. It was found that the saturation magnetization (M_s) increased and the Curie point decreased slightly with the increase of the amount of Er^{3+} substituted for gadolinium.

In [15,16], in order to obtain ferrite-garnets, the gel is uniformly distributed on an appropriate basis by the centrifugation and then calcined. In another work [17], the rare earth ferrite-garnet thin films were grown on crystal-oriented substrates in vacuum.

In [18] $Er_3Fe_5O_{12}$ was synthesized by citrate–nitrate gel combustion method and characterized by XRD. The isobaric molar heat capacity of this oxide was determined by differential scanning calorimetry method at temperatures ranging from 130 to 860 K. In the temperature range from 530 K to 560 K, the heat capacity shows an anomaly similar to the λ-type transition, which corresponds to a second-order phase transition and involving the magnetic order–disorder transition from ferromagnetic state to the paramagnetic state. The Curie temperature ($T_c = 544$ K) of $Er_3Fe_5O_{12}$ was determined by differential scanning calorimetry (DSC).

The physical properties of ferrite-garnets don't normally depend much on the above production methods, and the replacement of the rare earth element cation and/or the iron ion with the trivalent cations (the chemical defects) allows us to control the physical properties within the narrow limits [7–14,19].

However, the technological method (mechanical activation) for controlling the physical properties of any crystalline bodies has been widely used recently. This method consists in the targeted introduction of the structural defects (the dislocations and point defects) into crystalline bodies. It makes it possible to change both the concentration of the structural defects and their type in the crystalline bodies. In this case, the stoichiometry of the compositions does not change. This work is devoted to this method, and its purpose is to control the physical properties of the synthesized erbium ferrite-garnet by the mechanical force action combined with the shear deformation.

Materials and methods

The stoichiometric amounts of Fe and Er oxides ($Fe_2O_3 \geq 99.0\%$, $Er_2O_3 \geq 99.9\%$, Sigma-Aldrich) were mixed in the agate mortar for 2 h in the presence of ethanol. The resulting composition was dried in the thermostat at 200 °C in order to remove moisture. Next, the dried composition was pressed into a cylinder of 5 mm high and 10 mm in diameter for the subsequent synthesis in the high-temperature furnace. During the synthesis, the sample was placed into a platinum crucible with a lid. The synthesis was performed at 1200 °C. In 4 h, the furnace was cooled by inertia to room temperature. The synthesized cylindrical sample was ground in the agate mortar in the presence of ethanol, and the resulting powder was dried at 200 °C. Synthesized $Er_3Fe_5O_{12}$ was further ground into powder and studied on the Bruker D2 PHASER X-ray diffractometer, which uses Cu K_α ($K_{\alpha 1} = 1.54060$ Å and $K_{\alpha 2} = 1.54443$ Å) radiation, with the 2θ step of 0.01° and the aqcuisition time of 0.1 s per point. The Rietveld crystal structure was refined using the FullProf Suite 2000 software. The diffraction pattern showed the presence of an insignificant concentration of the α-Fe_2O_3 phase. Next, the $Er_3Fe_5O_{12}$ powder was mechanically activated between the Bridgman anvils at a fixed shear strain and various uniaxial pressures, while the lower anvil rotated at a speed of 3 rph. The number of the rotations was equal to two. Each of seven portions of the powder was pressed under the fixed pressure but for the next set of portions the pressure was increased by 40 MPa. The upper limit of the mechanical activation pressure was 320 MPa, which made it possible to avoid significant amorphization of the composition or the formation of the high-pressure phases. The parameter ζ, characterizing a shear deformation was determined to be equal to 12 by the formula:

$$\zeta = ln(vr/d) \tag{2}$$

where v is the rotation angle, r is the radius of the anvil, d is the thickness of the sample.

All the mechanically activated powders were studied using an electron microscope and a diffractometer. From seven parts of the mechanically activated ErIG powder, one sample 10 mm in diameter and about 1 mm thick was pressed at 2000 N for the further sintering in a high-temperature furnace. All the samples were sintered together at 1200 °C for 2 h. The density of the ceramic samples ranged from 6.65 to 6.80 g/cm^3, depending on the mechanical activation pressure. For the dielectric measurements, the silver paste was applied on the surface of the disks and then it was being burned into the surface at 750 °C for 20 min. The dielectric properties were analyzed by the E7-20 automatic immitance meter produced at the Minsk R&D Institute of Instrument Making (MNIPI, Belarus). The optical absorption spectra were studied at room temperature with the Shimadzu UV-2600 two-beam IR spectrophotometer. The thermal capacity of the samples in the shape of the 4 mm diameter discs was evaluated with the DSC 204 F1 Phoenix scanning calorimeter (Netzsch) in the temperature range from the ambient temperature to 750 K. The heating rate was 5 K min^{-1} with the measurement accuracy not exceeding 3%. The microstructure of the samples was observed and examined by transmission electron microscope EVO40 XVP (Karl Zeiss).

The magnetic properties at room temperature were studied with the LakeShore VSM 7404 vibration magnetometer.

Results and discussion

Structural characterization

To visualize the structural changes, all the samples that had undergone the mechanical activation after the synthesis were studied with the electron microscope. Fig. 1 shows the electron micrographs of the starting (a) and one of the mechanically activated (b) powder samples of ErIG. After the mechanical activation, all the powder samples were characterized by the presence of a "coat" of the fine particles on the
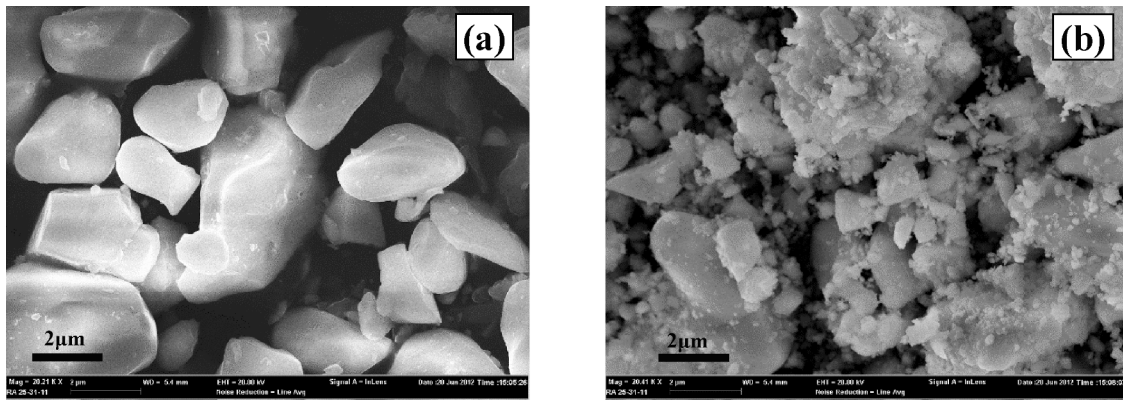
Fig. 1. The electron micrographs of the starting (a) and mechanically activated (b) $Er_3Fe_5O_{12}$ powders at 80 MPa.

surface of the larger particles. The relaxation of the mechanical energy supplied to the Bridgman anvils occurs through the various channels [20], two of which will be considered in this work: the first channel is the accumulation of the structural defects in the crystallites; the second one is the particle dispersion.

The recrystallization, as a result of which "the healthier grains" absorb "the less healthy grains" occurs in the process of the mechanical activation at certain pressures in the activated sample due to the ballistic diffusion. Structurally, the latter differ from the former by the higher concentration of the structural defects. However, at the higher pressures and other magnitudes of the shear deformations, "the healthy grains" can be dispersed again.

The structural perfection of the crystalline bodies and the dislocation density in them can be determined by the broadening of the X-ray diffraction profiles. This makes it possible to estimate the size of the coherent scattering regions, (D) and the value of the microstrains ($\Delta d/d$). However, the determination of the size of the mechanically activated particles by the Scherrer formula leads to the incorrect results, since this formula does not take into account the contribution of $\Delta d/d$ and the small size of the particles to the broadening of the profiles. Therefore, the separation of the D and $\Delta d/d$ contributions to the broadening of the diffraction profiles for the mechanically activated samples is a mandatory procedure. For this purpose, the approximation method which is well described in literature [21], was used in this work. The graphs of the dependence of D and $\Delta d/d$ on the mechanical activation pressure of the ErIG powder samples are shown in Fig. 2.Fig. 3.

The estimation of the dislocations density, ρ_D (Table 1), assuming that they are distributed chaotically, was performed according to the formula:

$$\rho D = 3nD^{-2} \tag{3}$$

where D is the size of the coherent scattering regions. The network of the dislocations, in which the dislocation coincides with each edge of the block, corresponds to the case when $n = 1$; the distance between the dislocations is maximal and the interaction is minimal.

As can be seen from Fig. 2, with an increase in the mechanical activation pressure to 80 MPa, the value of the microstrain increases abruptly, which is caused by an increase in the concentration of the dislocations. With a further increase in the activation pressure to 240 MPa, the microstrains change insignificantly, the concentration of the point defects increases, the concentration of the generated dislocations also increases, and the value of D reaches its minimum. This means that for the given parameters of the mechanical activation, a decrease in the size of D below 50 nm is highly doubtful. At the same time, the concentration of the point defects cannot grow if the pressure is more than 240 MPa. An increase in D and a decrease in $\Delta d/d$ observed at the activation pressure of 280 MPa are due to the dynamic recrystallization process and the absorption of the "weak" crystallites by the "healthier" crystallites. We had previously observed such an effect upon the mechanical activation of the ferroelectrics-relaxors and ferroelectromagnets, but at other pressures [21–23].

A thorough study of the X-ray diffraction patterns of the starting and mechanically activated $Er_3Fe_5O_{12}$ powders has shown that after the mechanical activation the crystalline structure of powders depending on the pressures is in different metastable states. The broadening of the Bragg maxima profiles, their shift along the diffraction angle scale, an increase in the background, and a change in the integral intensity correspond to this. As a confirmation of the above, Fig. 2 shows the diffraction profiles of the starting and mechanically activated powders at 160 MPa. The insets show the magnified reflection profiles from the plane (4 4 4).

Fig. 4 shows the dependence of the unit cell parameter on the pressure applied during the mechanical activation of the powders.

The behavior of the unit cell parameter is non-monotonic, and its oscillation in the pressure range 80–200 MPa is possibly due to the incomplete generation of dislocations and the active phase of the point defects generation.

Dielectric properties

Earlier in the work [24] the measurements of the dielectric constant, $\varepsilon'(T)$, and the dielectric losses, $tg\delta$, were performed in the region of glow temperatures, and the anomalies, ε', were found in the temperature range 110–80 K and $tg\delta$ at 45 K.

The authors compared the observed anomalies with the temperature measurements of the magnetic susceptibility, $\chi(T)$. The authors associated the anomaly in the range 110–80 K with a decrease in the magnetic
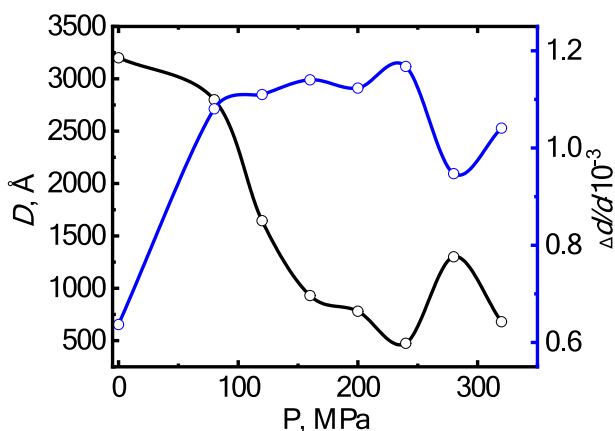

Fig. 2. The dependence of the sizes of the coherent scattering regions, D, and the microstrains, $\Delta d/d$, of the $Er_3Fe_5O_{12}$ powders on the mechanical activation pressure.
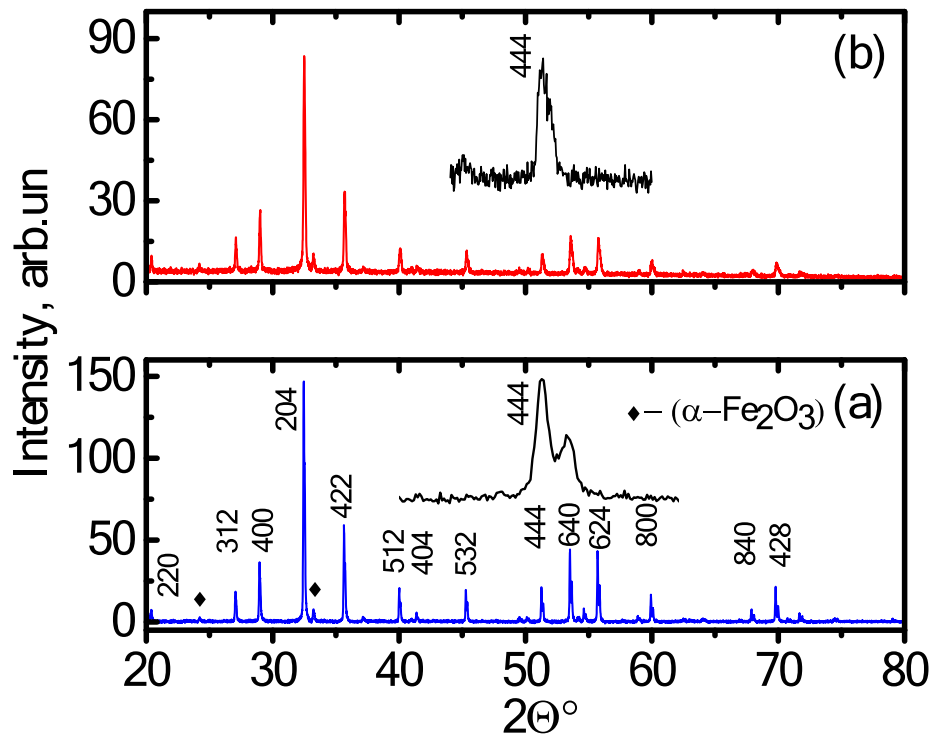
Fig. 3. The diffraction patterns of the starting (a) and mechanically activated (b) $Er_3Fe_5O_{12}$ powders at a pressure of 160 MPa.

Table 1
The values of the dislocation density of $Er_3Fe_5O_{12}$.

P, MPa	0	80	120	160	200	240	280	320
$\rho_D \cdot 10^9$, cm^{-2}	3	4	11	35	49	133	17	65

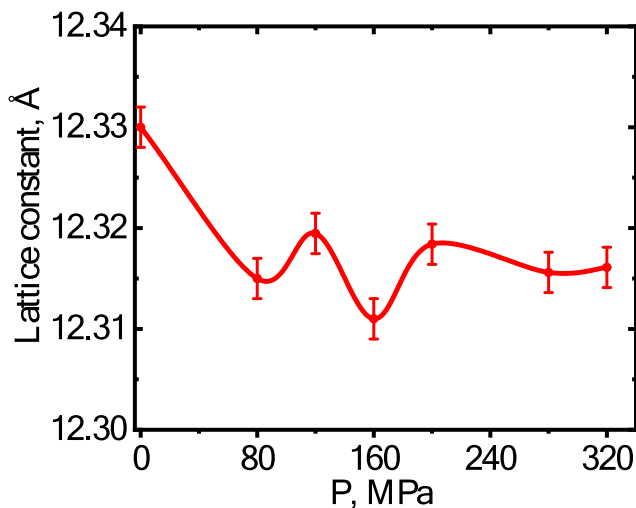**Fig. 4.** The dependence of the unit cell parameter of the $Er_3Fe_5O_{12}$ powders on the mechanical activation pressure.

susceptibility up to the compensation temperature T_c equal to 75 K. A noncollinear "umbrella" magnetic structure appears below this temperature. The change in the unit cell parameter corresponds to the ε' anomaly observed in the same temperature range. The $tg\delta$ anomaly at 45 K corresponds to the temperature below which the irreversibility occurs between the zfc and fc curves. The authors of [24] also concluded that the anomalies on the $\varepsilon'(T)$ dependence observed above T_c are insensitive

to the external magnetic field.

To sum up, the measurements of the dielectric properties were studied mainly at the negative temperatures. Therefore, despite the fact that ErIG has a cubic symmetry at room and higher temperatures, it was of interest to study the temperature dependences of ε and $tg\delta$ for the mechanically activated ErIG ceramics above room temperature.

Fig. 5 shows the graphs of $\varepsilon(T)$ and $tg\delta(T)$ dependences obtained at different frequencies of the measuring field of the starting (Fig. 5a, Fig. 5a') and mechanically activated (Fig. 5b, Fig. 5b') powders at 80 MPa of $Er_3Fe_5O_{12}$ ceramics.

As Fig. 5(a) and (Fig. 5 (b) indicate, the anomalies are found at $T =$ 212 °C. An additional anomaly with a relaxor behavior of the $\varepsilon(T)$ dependence is characteristic for a mechanically activated sample at $T =$ 363 °C, (see Fig. 5 (b)). Such a behavior of $\varepsilon(T)$ turned out to be characteristic of all the mechanically activated ceramic ErIG samples studied in this work. However, none of the temperatures at which the $\varepsilon(T)$ anomalies are observed corresponds to the Néel temperature, T_N. According to [14,24], the Néel temperature of ErIG is $T_N = 564.9$ and 560 K, respectively, and for all our mechanically activated samples T_N is located to the right of the first $\varepsilon(T)$ anomaly. The first maximum is observed approximately at $T = 317$ °C for the starting sample and $T =$ 292 °C for the mechanically activated sample at 80 MPa (see Fig. 5 (a') and Fig. 5 (b')). The anomaly observed at $T = 212$ °C is due to the thermal depletion of the impurity energy levels. To verify this assumption, we studied the $\varepsilon(T)$ dependences of the several mechanically activated samples both upon heating and upon cooling. During the reverse run (cooling), this anomaly did not appear on the $\varepsilon(T)$ dependence.

Optical spectra

The band gap (E_g) is one of the parameters that are commonly called fundamental in condensed matter physics. This parameter classifies all crystalline bodies into metals, semiconductors and dielectrics. However, this parameter depends on many factors, including the structural perfection of the crystalline body. Since the mechanically activated ErIG samples are disordered structures to some extent, it is of interest to study
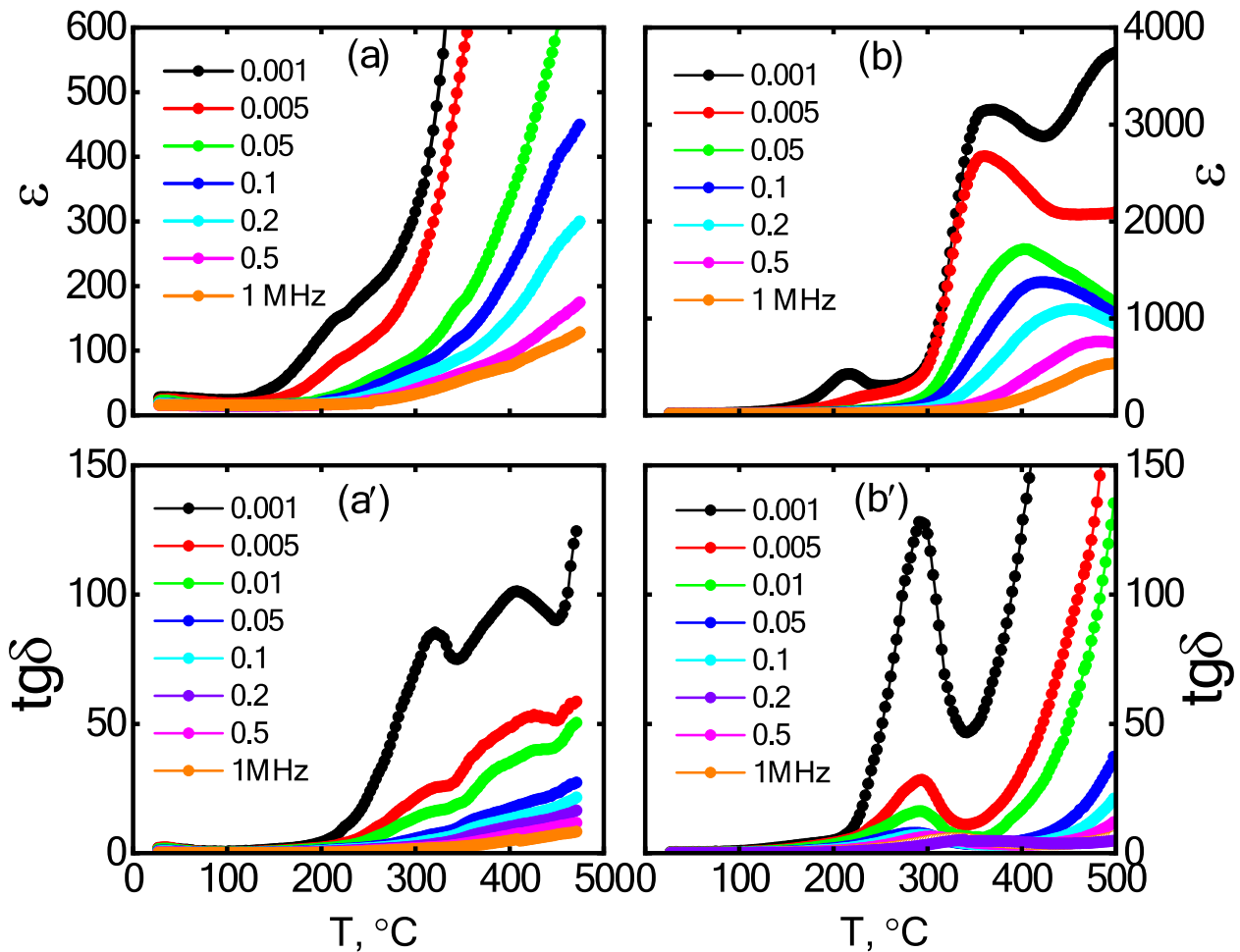
Fig. 5. The temperature dependences of ε and $tg\delta$ of the starting (a), (a') and mechanically activated (b), (b') powders of $Er_3Fe_5O_{12}$ ceramics at 80 MPa.

the effect of the mechanical activation on E_g. For this purpose, the intrinsic optical absorption of the starting and mechanically activated samples was studied. Based on the spectral shape of the reflection coefficient $R(\lambda)$ obtained at room temperature, the Kubelka-Munk function was calculated, which is proportional to the ratio of the absorption coefficient α and the scattering coefficient s of an infinitely thick opaque sample [25]:

$$F(R) = (1 - R)^2/2R = \alpha/s \tag{4}$$

To estimate the band gap, the equation proposed by Tauk, Davis, and Mott [26–28] can be used:

$$(h\nu\,\alpha)^{1/n} = A(h\nu - E_g) \tag{5}$$

where h is Planck's constant, ν is frequency, and A is proportionality coefficient.

The value of the exponent n indicates the nature of the transition. It is known that $n = 1/2$ is true for direct allowed transitions, and $n = 2$ for the indirect allowed transitions. It is possible to determine the nature of the interband transitions by substituting these quantities into the equation (5) and analyzing the absorption edge. For the allowed direct transitions ($n = 1/2$), the resulting reflectance spectrum is converted to the Kubelka-Munk function. Thus, the vertical axis is converted to the $F(R_\infty)$ value, which is proportional to the absorption coefficient. The proportionality coefficient A in the Tauk equation is replaced by $F(R_\infty)$. Then the working equation is:

$$(h\nu\cdot F(R_\infty))^2 = A(h\nu - E_g) \tag{6}$$

Further, using the Kubelka-Munk function $(h\nu\cdot F(R_\infty))^2$ the $(E\cdot F(R_\infty))^2$ dependences were constructed as the function of $h\nu$. The corresponding graphs for two samples are shown in Fig. 6. The point of the intersection of the tangent to the straight sections with the abscissa determines the width of the band gap E_g. As can be seen from Fig. 6, the absorption characteristics of the starting (Fig. 6a and Fig. 6a') and mechanically activated samples at 200 MPa (Fig. 6b and Fig. 6b') differ. The ErIG starting sample has more impurities than the mechanically activated samples do. In the latter, the effective diffusion coefficient during the mechanical activation increases many times. The activation energy of the diffusion processes decreases and most of the impurities during the process of sintering migrate to the crystallite surface and into the atmosphere. The values of the E_g energies calculated from the absorption (reflection) spectra of the starting and mechanically activated ErIG ceramic samples at room temperature are shown in Table 2.

As can be seen from Fig. 6 and Table 2, the mechanical activation of ErIG leads to a noticeable change in the reflection spectrum and an increase in the band gap.

Heat capacity of the $Er_3Fe_5O_{12}$ ceramics

The study of the phase transitions and structural changes based on the temperature dependences of the heat capacity of crystalline bodies is a nondissipative method that does not induce the additional phase transitions. Previously, such measurements were performed in [29] in the temperature range from 5 to 210 K. However, the high-temperature region remains poorly studied so far. Below we present the measurement results for three ceramic samples, two of which were obtained from the
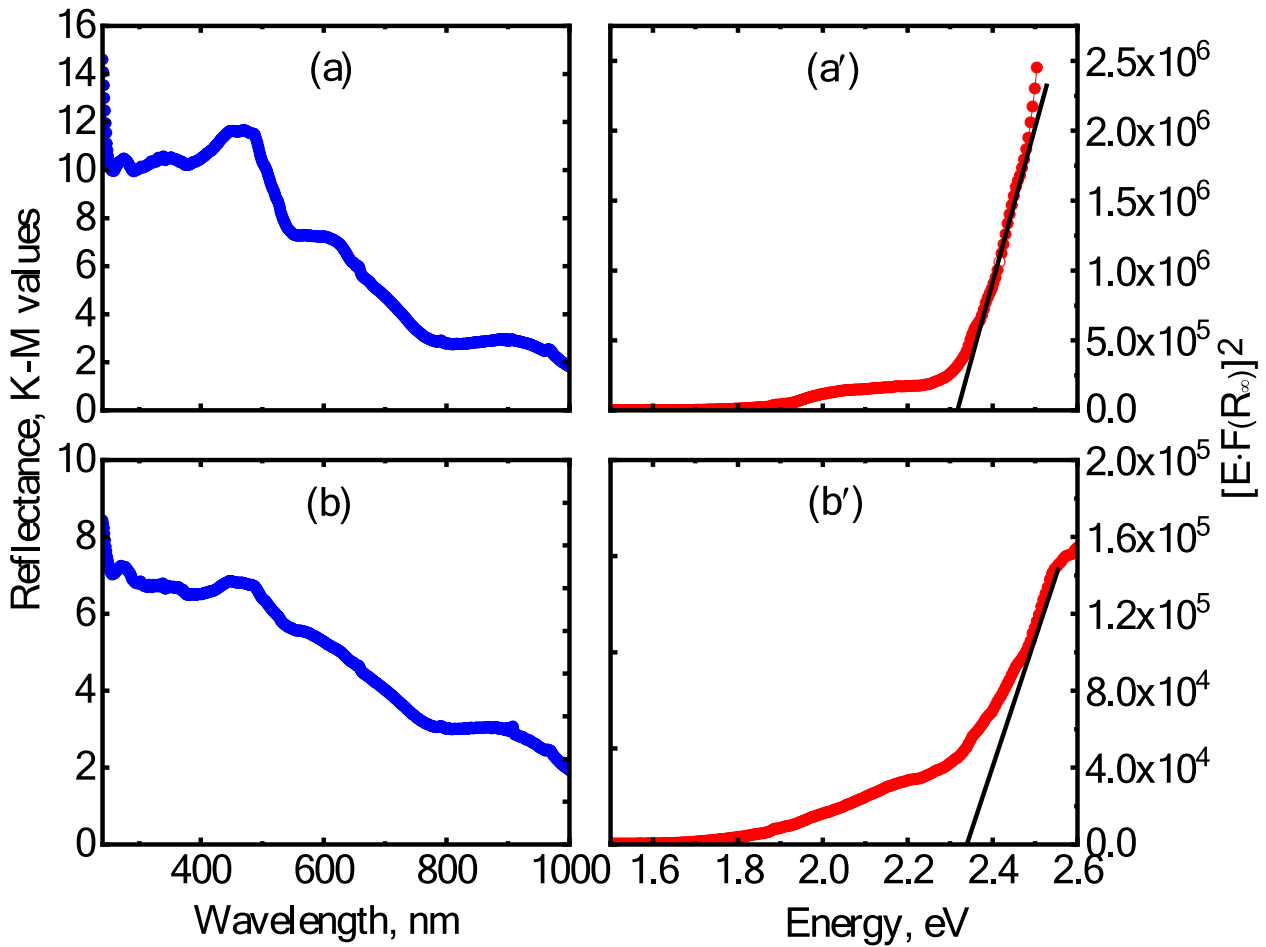
Fig. 6. The dependence of the absorption coefficient by Kubelka-Munk function on the wavelength and function $(E \cdot F(R_\infty))^{-2}$ on the energy, E, of the starting (a, a′) and mechanically activated (b, b′) powders of the $Er_3Fe_5O_{12}$ ceramics at 200 MPa.

Table 2
The dependence of the energy of the $Er_3Fe_5O_{12}$ band gap on the mechanical activation pressure.

P, MPa	0	80	120	160	200	280	320
E_g, eV	2.3	2.33	2.44	2.45	2.34	2.43	2.45

mechanically activated ErIG powder.

As can be seen from Fig. 7, the anomaly λ, which is also observed on the ε temperature dependence in the shape of a "dome", is found on the temperature dependence of the capacity C_p of the starting sample (curve 1) at the temperature of the antiferrimagnetic to paramagnetic transition $T_N \approx 542$ K.

The mechanical activation leads to the smearing of the antiferrimagnetic to paramagnetic transition and the noticeable increase in C_p in a wide temperature range (by 5–10%) and the shift in the T_N temperature to the low-temperature region by $\Delta T \approx 10$ K ($T_N \approx 532$ K) at 120 MPa (curve 3) and $\Delta T \approx 24$ K ($T_N \approx 518$ K) at 200 MPa (curve 2). This behavior is due to the fact that the mechanical activation leads to the high concentration of the point defects and dislocations in the nanostructured ceramics [30]. The high concentration of the defects [23] and the deformation field created by the dislocations [31] can significantly affect the features of the thermodynamic values of the sample in the region of the phase transition. According to [23], the high concentration of the defects can lead to the increase in the heat capacity and the smearing of the thermodynamic properties in the phase transition region, which is observed in the experiment. It was shown in [31]
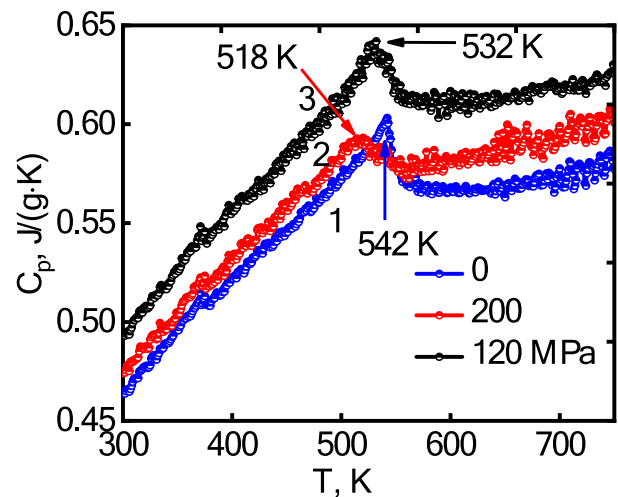

Fig. 7. The thermal dependence of the heat capacity of the $Er_3Fe_5O_{12}$ ceramics obtained from the starting (1) and activated powders at 200 (2) and 160 (3) MPa.

that the ordered regions near the dislocation lines can appear at much higher temperatures than the transition temperature in an "ideal" crystal. The ordered regions form a complex random framework that consists of the ordered domains (electric or magnetic) in the various crystallites and penetrates the entire crystal, although occupying a small

fraction of its volume. The correlation length of such regions is very short. At $T > T_N$, such a structure can be transformed into a state with a predominant number of the domains with a certain polarization sign or magnetization direction, i.e., a phase transition takes place in the dislocation framework. With decreasing the temperature, the thickness of the ordered regions of the framework grows, and at $T = T_N$ the comparatively large ordered clusters should appear, capturing many dislocations. As a result, ordering extends to the entire volume of the crystal in the region $T \approx T_N$, and this process should manifest itself as a diffuse second-order phase transition in the experiment. Thus, the experimentally observed diffuse phase transition of nanostructured ErIG is due to a high concentration of the point defects, the formation of a dislocation framework, and the crystallite boundaries. The shift of the phase transition of the mechanically activated sample to the low temperature region can be associated with a decrease in the crystallite size (size effect [32,33]).

Magnetic properties

Magnetization measurements of the polycrystalline $Er_3Fe_5O_{12}$ samples were performed at room temperature. Fig. 8 (a) shows the hysteresis loops of the starting and mechanically activated powder samples. It can be seen from the hysteresis loops that they do not saturate under the applied magnetic fields, therefore, the change in the magnetization was estimated along the tangent drawn to the curve up to the intersection with the $M(H)$ axis, and by its residual value, M_r directly from the curves (see Fig. 8 (b)).

Fig. 8 (b) shows that, in comparison with the starting sample, the value of M_r and the coercive force H_c of the mechanically activated samples increase. However, this growth is not monotonic, which is due to the different structural states of the samples. The dislocations and point defects generated in the process of the mechanical activation significantly affect the transformation of the sample into a magnetically ordered state homogeneous throughout the volume. The interaction of the domain structure with the crystal lattice defects ultimately determines the structure-sensitive properties of the ErIG samples, which is true to any magnetic materials.

Conclusion

In this work, the ferrite garnet $Er_3Fe_5O_{12}$ has been synthesized by the solid-phase reaction method. Then, mechanically activated powder samples in various metastable states, have been obtained from the pre-synthesized powder by using Bridgman anvils, from which the ceramic samples have been subsequently prepared. X-ray diffraction studies have shown that the unit cell parameters of mechanically activated samples decrease in comparison with the starting sample. It was shown by dielectric measurements of ceramics that $Er_3Fe_5O_{12}$ is characterized by a relaxor behavior of dielectric polarization, and an anomaly is observed in the forward run of the $\varepsilon(T)$ dependence in the vicinity of $T = 212\,°C$, which is caused by thermal depletion of impurity energy levels.

The band gap has been calculated for each ceramic sample by measuring the optical absorption spectra. The band gap depends on the amount of pressure applied during mechanical activation.

The temperature dependence of the heat capacity C_p of the starting and mechanically activated samples is characterized by λ – an anomaly corresponding to the phase transition temperature T_N from antiferrimagnetic to paramagnetic state; moreover, for mechanically activated samples, it shifts to the low temperature region.

By measuring the magnetic hysteresis loops $M(H)$, it was determined that the coercivity H_c and remanence M_r of mechanically activated samples are higher than the starting sample. This phenomenon is conditioned by different sizes and morphology of crystallites after mechanical activation under different pressures, and by different concentrations and types of structural defects in the crystallites of mechanically activated powders.

As the result these complex studies bring us that the structural defects generated during mechanical activation are a mechanism that controls the physical parameters of $Er_3Fe_5O_{12}$.

CRediT authorship contribution statement

K.G. Abdulvakhidov: Data curation, Writing - original draft. **A.V. Soldatov:** Funding acquisition, Methodology, Supervision. **I.P. Dmitrenko:** Resources, Software, Writing - review & editing. **Li Zhengyou:** Resources, Software, Writing - review & editing. **S.N. Kallaev:** Conceptualization, Writing - review & editing. **Z. Omarov:** Conceptualization, Writing - review & editing.
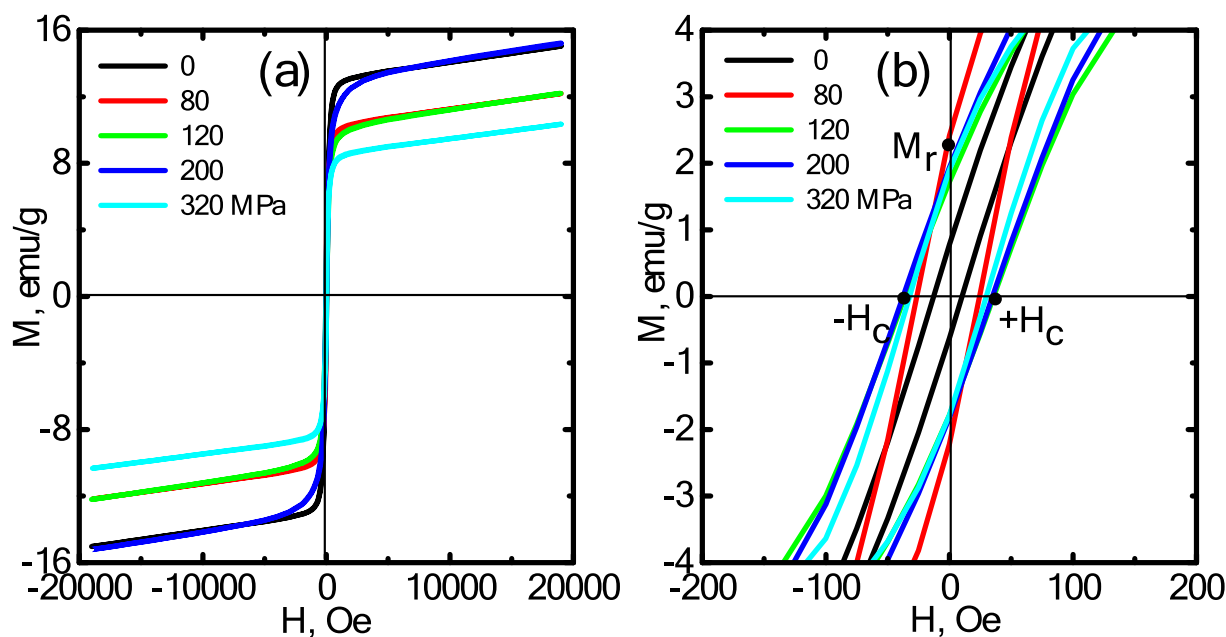

Fig. 8. The hysteresis loops curve of $Er_3Fe_5O_{12}$ (a) and their parameters (b).

Declaration of Competing Interest

The authors declare that they have no known competing financial interests or personal relationships that could have appeared to influence the work reported in this paper.

Acknowledgements

References

[1] Geller S, Gilleo MA. The crystal structure and ferrimagnetism of yttrium-iron garnet, $Y_3Fe_2(FeO_4)_3$. J Phys Chem Solids 1957;3(1-2):30–6. https://doi.org/10.1016/0022-3697(57)90044-6.

[2] Pauthenet R. The magnetic properties of yttrium and rare earth ferrites with the formula $5Fe_2O_3.3M_2O_3$. Ann Phys (Paris) 1958;13:424–62. https://doi.org/10.1051/anphys/195811030424.

[3] Geller S, Gilleo MA. Structure and ferrimagnetism of yttrium and rare-earth–iron garnets. Acta Cryst 1957;10(3):239. https://doi.org/10.1107/S0365110X57000729.

[4] Néel ML. Magnetic properties of ferrites; ferrimagnetism and antiferromagnetism. Ann Phys (Paris) 1948;12:137–98. https://doi.org/10.1051/anphys/194812030137.

[5] Gilleo MA. Chapter 1 Ferromagnetic insulators: Garnets. Handb. Ferromagn. Mater., vol. 2, Elsevier; 1980, p. 1–53. https://doi.org/10.1016/S1574-9304(05)80102-6.

[6] Brabenec M, Englich J, Novak P, Lütgemeier H. On the transferred hyperfine interaction in substituted yig. Hyperfine Interact 1987;34(1-4):459–61. https://doi.org/10.1007/BF02072756.

[7] Ristić M, Popović S, Musić S, Czakó-Nagy I, Vértes A, Maiorov M, Petrov A. Formation and properties of oxide phases in the system Er_2O_3-Fe_2O_3. J Alloy Compd 1997;256(1-2):27–33. https://doi.org/10.1016/S0925-8388(96)02951-9.

[8] Xu HK, Sorensen CM, Klabunde KJ, Hadjipanayis GC. Aerosol synthesis of gadolinium iron garnet particles. J. Mater. Res. 1992;7(3):712–6. https://doi.org/10.1557/JMR.1992.0712.

[9] Matsumoto K, Yamaguchi K, Ueno A, Fujii T. Preparation of Bi-Substituted YIG Garnets by Sol-Gel Synthesis and Their Magnetic Properties. IEEE Transl. J. Magn. Jpn. 1991;6(1):15–22. https://doi.org/10.1109/TJMJ.1991.4565101.

[10] Opuchovic O, Kareiva A, Mazeika K, Baltrunas D. Magnetic nanosized rare earth iron garnets $R_3Fe_5O_{12}$: Sol–gel fabrication, characterization and reinspection. J Magn Magn Mater 2017;422:425–33. https://doi.org/10.1016/j.jmmm.2016.09.041.

[11] Shaiboub R, Ibrahim NB, Abdullah M, Abdulhade F. The Physical Properties of Erbium-Doped Yttrium Iron Garnet Films Prepared by Sol-Gel Method. Journal of Nanomaterials 2012;2012:1–5. https://doi.org/10.1155/2012/524903.

[12] Bsoul I, Olayaan R, Lataifeh M, Mohaidat QI, Mahmood SH. Structural and magnetic properties of $Er_3Fe_{5-x}Ga_xO_{12}$ garnets. Mater Res Express 2019;6. https://doi.org/10.1088/2053-1591/ab198b.

[13] Zheng J, Fu Q, Chen X, Chakrabarti C, Wang P, Yin H, et al. Colossal dielectric response in erbium iron garnet ceramics. J Mater Sci Mater Electron 2020. https://doi.org/10.1007/s10854-020-04775-9.

[14] Mohaidat QI, Lataifeh M, Mahmood SH, Bsoul I, Awawdeh M. Structural, Mössbauer Effect, Magnetic, and Thermal Properties of Gadolinium Erbium Iron Garnet System $Gd_{3-x}Er_xFe_5O_{12}$. J Supercond Nov Magn 2017;30(8):2135–41. https://doi.org/10.1007/s10948-017-4003-y.

[15] Kojima K, Mizukami F, Miyazaki M, Maeda K. Selective formation of thin film iron garnet by complexing agent-assisted sol-gel processing. J Non-Cryst Solids 1992; 147-148:442–6. https://doi.org/10.1016/S0022-3093(05)80655-6.

[16] Matsumoto K, Yamaguchi K, Fujii T, Ueno A. Preparation of bismuth-substituted yttrium iron garnet powders by the citrate gel process. J Appl Phys 1991;69(8): 5918–20. https://doi.org/10.1063/1.347815.

[17] Alex M, Shono K, Kuroda S, Koshino N, Ogawa S. Ce-substituted garnet media for magneto-optic recording. J Appl Phys 1990;67(9):4432–4. https://doi.org/10.1063/1.344922.

[18] Parida SC, Rakshit SK, Singh Z. Heat capacities, order–disorder transitions, and thermodynamic properties of rare-earth orthoferrites and rare-earth iron garnets. J Solid State Chem 2008;181(1):101–21. https://doi.org/10.1016/j.jssc.2007.11.003.

[19] Sayetat F. Huge magnetostriction in $Tb_3Fe_5O_{12}$, $Dy_3Fe_5O_{12}$, $Ho_3Fe_5O_{12}$, $Er_3Fe_5O_{12}$ garnets. J Magn Magn Mater 1986;58(3-4):334–46. https://doi.org/10.1016/0304-8853(86)90456-7.

[20] Boldyrev V. Mechanochemistry and mechanical activation of solids. Solid State Ionics 1993;63–65:537–43. https://doi.org/10.1016/0167-2738(93)90157-X.

[21] Abdulvakhidov KG, Sirota MA, Budnyk AP, Lastovina TA, Abdulvakhidov BK, Sadykov SA, et al. The role of defects in the physical properties of mechanically activated $PbTiO_3$ ferroelectrics. J Phys Condens Matter 2019;31. https://doi.org/10.1088/1361-648X/aafebe.

[22] Sirota MA, Abdulvakhidov KG, Budnyk AP, Soldatov AV, Bugaev AL, Lastovina TA, et al. Mechanical activation and physical properties of $Pb(Zr_{0.56}Ti_{0.44})O_3$. Ferroelectrics 2018;526:1–8. https://doi.org/10.1080/00150193.2018.1456130.

[23] Abdulvakhidov KG, Sirota MA, Budnyk AP, Lastovina TA, Soldatov AV, Kallayev SN, et al. The influence of mechanical activation on the dielectric and dynamic properties and structural parameters of the solid solution of $Pb(Zr_{0.56}Ti_{0.44})O_3$. Mater Res Express 2018;5:115029. https://doi.org/10.1088/2053-1591/aaded3.

[24] Maignan A, Singh K, Simon Ch, Lebedev OI, Martin C, Tan H, Verbeeck J, Van Tendeloo G. Magnetic and magnetodielectric properties of erbium iron garnet ceramic. J Appl Phys 2013;113(3):033905. https://doi.org/10.1063/1.4776716.

[25] Kortüm G, Braun W, Herzog G. Principles and Techniques of Diffuse-Reflectance Spectroscopy. Angew. Chem. Int. Ed. Engl. 1963;2(7):333–41. https://doi.org/10.1002/anie.196303331.

[26] Tauc J, Grigorovici R, Vancu A. Optical Properties and Electronic Structure of Amorphous Germanium. phys. stat. sol. (b) 1966;15(2):627–37. https://doi.org/10.1002/pssb.19660150224.

[27] Wooten F. Absorption and dispersion. In: Wooten FBT-OP of S, editor. Opt. Prop. Solids, Elsevier; 1972, p. 42–84. https://doi.org/10.1016/B978-0-12-763450-0.50008-8.

[28] Davis EA, Mott NF. Conduction in non-crystalline systems V. Conductivity, optical absorption and photoconductivity in amorphous semiconductors. Phil Mag 1970; 22(179):0903–22. https://doi.org/10.1080/14786437008221061.

[29] Guillot M, Tcheou F, Marchand A, Feldmann P, Lagnier R. Specific heat in Erbium and Yttrium Iron garnet crystals. Z. Physik B - Condensed Matter 1981;44(1-2): 53–7. https://doi.org/10.1007/BF01292652.

[30] Abdulvakhidov KG, Kallaev SN, Kazaryan MA, Plyaka PS, Sadikov SA, Sirota MA, et al. Nanostructured $SmFeO_3$ electrophysical properties. IOP Conf. Ser. Mater. Sci. Eng., 2016;112:012020. https://doi.org/10.1088/1757-899X/112/1/012020.

[31] Kallaev SN, Alikhanov N- M-R, Omarov ZM, Sadykov SA, Sirota MA, Abdulvakhidov KG, Soldatov AV. Thermodynamic Properties and Phase Transitions of Microcrystalline and Nanostructured $SmFeO_3$ Ceramics. Phys. Solid State 2019;61(7):1300–3. https://doi.org/10.1134/S1063783419070126.

[32] Lin S, Lü T, Jin C, Wang X. Size effect on the dielectric properties of $BaTiO_3$ nanoceramics in a modified Ginsburg-Landau-Devonshire thermodynamic theory. Phys Rev B 2006;74:134115. https://doi.org/10.1103/PhysRevB.74.134115.

[33] Kallaev SN, Omarov ZM, Bakmaev AG, Abdulvakhidov K. Heat capacity of nanostructured $BaTiO_3$ ceramics. Phys. Solid State 2013;55(5):1095–7. https://doi.org/10.1134/S1063783413050144.